Journal of Materials Science: Materials in Electronics (2020) 31:13150–13157
https://doi.org/10.1007/s10854-020-03866-x

Magnetic and structure property correlations in Mn-doped $BiFeO_3$ system

Mingyu Zhang[1] · Jia Liu[1] · Chaoyong Wang[1] · Xiaofeng An[1] · Yufei Wang[1] · Weiwei Xu[1] · Li Gu[2]

Received: 2 April 2020 / Accepted: 24 June 2020 / Published online: 23 July 2020

Abstract
In this paper, the synthesis of $BiFe_{1-x}Mn_xO_3$ ($x = 0.05, 0.10, 015, 0.20$) thin films using a sol–gel technique was proposed. The structural characteristics of the thin films were investigated by X-ray diffraction (XRD), indicating a structural transition from typical rhombohedral-*R*3*c* ($BiFeO_3$) to orthorhombic-*Pbmn* ($BiFe_{0.80}Mn_{0.20}O_3$). It was shown that, Mn was successfully doped into $BiFeO_3$ films and the Fe^{3+} ions in the films increased after doping by the X-ray photoelectron spectroscopy (XPS) analysis. The numerical results in this paper showed that the saturation magnetization of these $BiFeO_3$ thin films had been found to increase on doping with Mn^{2+} ions, reaching a maximum value of 83.5 emu/cm^3 for the $BiFe_{0.80}Mn_{0.20}O_3$ thin films. The numerical results also revealed that the proposed method in this paper can serve as a useful theoretical tool for gaining insight into the correlations of magnetic and structure property for $BiFeO_3$ thin films.

1 Introduction

Ideally, with the same pressure and temperature conditions, multiferroic materials exhibit three coupled ordering parameters, that is ferromagnetism, ferroelectricity, or ferroelasticity [1]. Due to its characteristics, it can be widely used in storage devices, sensors, and other products, multiferroic materials are studied in the recent years [2]. More attentions have been paid to the BiFeO, since it is the only one that has both magnetism and strongly ferroelectric properties at normal atmospheric temperature [3, 4]. The $BiFeO_3$ has the dual characteristics of ferroelectricity and ferromagnetism under the action of electric field, so it is a wider application prospect [5]. There are two difficulties in the preparation of $BiFeO_3$, one is the existence of oxygen vacancy, the other is the charge defect caused by the volatilization of Bi element, the charge defect will produce large leakage current in the film [6]. Therefore, how to improve the electrical properties of the film and reduce the leakage current is the key problem to the successful application of $BiFeO_3$ film. $BiFeO_3$ is a unique perovskite structure. Recently, doping technique is very popular. He et al. reported the mechanical strength between ZnS glass, and PbO-B_2O_3-ZnO powder can be significantly enhanced by doping the solder/braze by $PbTiO_3$ particles [7]. La, Sm, Nd, and other rare earth elements can be used to replace Bi position, to reduce oxygen vacancy, to stabilize oxygen octahedral structure, and to improve the structural stability of ferroelectric materials [6, 8, 9]. The transition metal ions such as Cu, Ti, Cr can replace the Fe site and further improve the magnetic spin structure of $BiFeO_3$, in order to improve the ferromagnetic properties of $BiFeO_3$ materials [10–12]. Sharma et al. studied that the $BiFe_{1-x}M_xO_3$ samples (M=Ni) exhibited a saturated M–H hysteresis loop (the saturation magnetization value Ms ~ 3.2 emu/g), and the improved ferromagnetic was attributed to the distortion of Fe–O–Ni bond angle [13]. According to Dutta et al., it is known that the enhanced magnetic properties of $Bi_{1-x}Sm_xFe_{1-y}Zr_yO_3$ (x, $y = 0, 0.02, 0.05$) nanorods were derived from the decrease of nanoparticle size and the increase of structural distortion caused by the doped ions entering the host lattice [14]. And it is noted that, the advantage of Mn-doped $BiFeO_3$ lies in that Mn possesses magnetic activity and the multivalent states of Mn ions enable the crystal to compensate for the charge. There are many reports on the multiferroic

Electronic supplementary material The online version of this article (https://doi.org/10.1007/s10854-020-03866-x) contains supplementary material, which is available to authorized users.

✉ Li Gu
guli@sziit.edu.cn

[1] School of Information Engineering, Jilin Engineering Normal University, Changchun 130052, China

[2] Sino-German School, Shenzhen Institute of Information Technology, Shenzhen 518172, China

properties of Mn-substituted $BiFeO_3$ ceramics and powders. Abushad et al. [15] reported the value of magnetization for the pristine sample is found to be 0.14 emu/g and enhances for 2% Mn-doped sample (0.16 emu/g). Homchenko et al. [16] revealed that containing about 17% of the polar phase at room temperature, possesses spontaneous magnetization (Ms ≈ 0.225 emu/g) exceeding that observed for the purely antipolar sample (Ms ≈ 0.185 emu/g). However, magnetic properties of Mn-doped $BiFeO_3$ thin films are rarely reported. Due to which the Mn possess magnetic, the replacement of Mn is expected to have a positive impact on the future application of specific multifunctional devices. Moreover, in the development of semiconductor technology, device miniaturization has always been the focus on research [17]. Therefore, we also focused on the observation of film thickness in our study. Thereafter, the method of substituting Mn ions in $BiFeO_3$ was adopted to prepare suitable materials considering from the technical point of view.

Motivated by the above-mentioned techniques, $BiFe_{1-x}Mn_xO_3$ ($x = 0.05$, 0.10, 015, 0.20) thin films were prepared by a sol–gel technique in the paper. The magnetic properties were investigated at normal atmospheric temperature and compared with the original $BiFeO_3$ thin films. By doping manganese to control $BiFeO_3$ magnetic properties, the effect of grain refinement, oxygen vacancy concentration, and ferromagnetic properties on the film were studied in this paper.

2 Experimental section

$BiFeO_3$, $BiFe_{0.95}Mn_{0.05}O_3$, $BiFe_{0.90}Mn_{0.10}O_3$, $BiFe_{0.85}Mn_{0.15}O_3$, and $BiFe_{0.80}Mn_{0.20}O_3$ precursor solutions were prepared by sol–gel method using $Bi(NO_3)_3{\cdot}5H_2O$, $Fe(NO_3)_3{\cdot}9H_2O$ and $Mn(NO_3)_2{\cdot}4H_2O$. Firstly, all nitrates were dissolved in glycol with a solution concentration of 0.2 mol/l and stirred at room temperature for 5 h. Secondly, the solution was dispersed on quartz and Si (100) substrates by spin coating. The film was deposited at 1000 rpm for 3 s and 4000 rpm for 30 s. After spin coating, each film was calcined at 350 °C for 10 min to decompose the remaining organic matter. Rotate the coating and the pyrolysis process 7 times until the required thickness. Finally, the dried thin films were annealed in an ambient atmosphere for 1 h under rapid heat treatment at 500 °C.

3 Characterization

The phase composition and structure of the films were characterized by XRD using Rigaku D/MAX 3C X-ray powder diffractometer under CuKα1 radiation ($\lambda = 1.5406$ Å). The X-ray diffraction data were analyzed by JADE 6.5 program, and the lattice parameters are obtained. The surface morphology and the interface contact of the films were measured to observe a field emission scanning electron microscope (FESEM). The microstructure properties were studied by transmission electron microscopy (TEM). The oxidation states of elements were analyzed by ESCALAB 250XI XPS. The magnetic hysteresis (M-H) loops were measured using the Lake Shore 7407 vibrating sample magnetometer (VSM) at normal atmospheric temperature.

4 Results and discussion

Figure 1a illustrates the XRD patterns of five kinds of $BiFeO_3$-based thin films, measured at normal atmospheric temperature. All the components have a rhombic structure of the spatial group R3C, and there is no secondary phase. Razad et al. reported that a small trace of secondary phases Bi25FeO39 and Bi2Fe4O9 observed along with the main phase ($BiFeO_3$) in BiFe0.975Ni0.025O3 sample due to the kinetics of formation [4]. The Bragg angle at 2θ of about 32° indexing to the rhombohedral structure, trend to merge and form single diffraction peaks with Mn doping content increasing. This indicates that the lattice distances of these planes decrease gradually due to variation of doping concentration and the radii of Fe^{3+} and Mn^{2+} ions and a structural transition of typical rhombohedral-*R3c* ($BiFeO_3$)

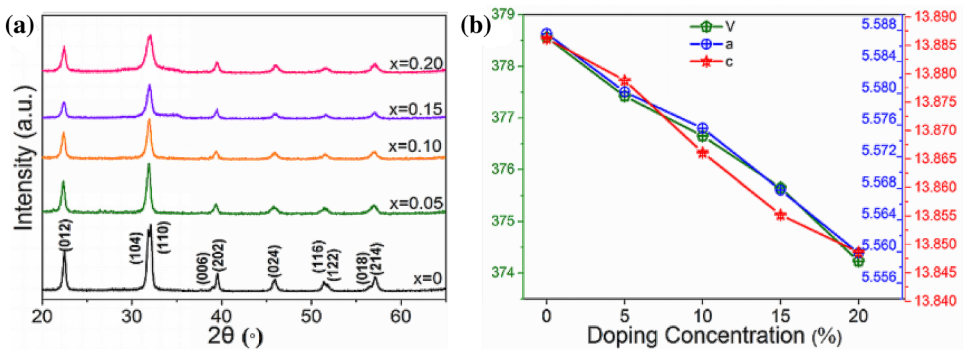

Fig. 1 XRD patterns of samples and lattice parameters and cell volumes. **a** XRD patterns of pure and doped $BiFeO_3$ thin films on Si substrates in the range of 2θ from 20° to 65°. **b** Calculated lattice parameters (**a**, **c**) and cell volumes (*V*) as a function of all samples

to orthorhombic-*Pbmn* ($BiFe_{0.80}Mn_{0.20}O_3$) [16]. The crystal structure details and lattice parameters of all samples extracted by Rietveld fine fitting in Fig. 1b. The smaller the ion radius and lattice parameter are, the greater the stress in the crystal structure is [15]. In addition, the quantitative relationship between the structural stability of the synthesized $BiFeO_3$ and the goldsmith tolerance factor (t) of perovskite is as follows, $t = (R_B + R_o)/\sqrt{2}(R_B + R_o)$ (R stands for the ionic radius of the respective element). The value of t is 0.8403, 0.8401, 0.8393, 0.8388, 0.8387 for $BiFeO_3$, $BiFe_{0.95}Mn_{0.05}O_3$, $BiFe_{0.90}Mn_{0.10}O_3$, $BiFe_{0.85}Mn_{0.15}O_3$ and $BiFe_{0.80}Mn_{0.20}O_3$ thin film, respectively. In this way, $t = 1$ corresponds to the ideal cubic structure, while $t < 1$ represents the compressive strain associated to the lattice mismatch between cations. In the current case, the estimated value of the tolerance, and the estimated tolerance factors of all samples are less than 0.9, which indicates that there are large deviations and distortions in the $BiFeO_3$ structure [18].

The morphology and homogeneity of the original samples are studied by SEM, $BiFe_{0.95}Mn_{0.05}O_3$, $BiFe_{0.90}Mn_{0.10}O_3$, $BiFe_{0.85}Mn_{0.15}O_3$, and $BiFe_{0.80}Mn_{0.20}O_3$ thin film and depicted in Fig. 2a–e. The particle size of doped $BiFeO_3$ film is smaller than that of un-doped $BiFeO_3$ film. The decrease of average particle size of doped samples may be due to the confinement of crystal growth caused by ion substitution with different radii [15]. The insets in Fig. 2 correspond to cross-sectional images of all films, respectively. From the observed image, we can see that the film adheres well to the substrate, and no cracks appear between the film and the substrate. In addition, the cross-sectional image determines the thickness of pristine, $BiFe_{0.95}Mn_{0.05}O_3$, $BiFe_{0.90}Mn_{0.10}O_3$, $BiFe_{0.85}Mn_{0.15}O_3$, and $BiFe_{0.80}Mn_{0.20}O_3$ thin film, which are estimated to be 428.90 nm, 414.81 nm, 396.09 nm, 370.31 nm and 220.31 nm, respectively. The thickness variation of Mn-doped film can be explained by suppressing the oxygen vacancy in the films, which causes the oxygen ion movement to slow down and reduce the grain growth rate [19]. The elemental mapping images of $BiFeO_3$ and $BiFe_{0.80}Mn_{0.20}O_3$ are recorded to study the distribution of elements in the nanostructures (Supplementary Figure. S1). These images showed that Bi, Fe, and O are uniformly distributed in the $BiFeO_3$ solution. Mn elemental mapping

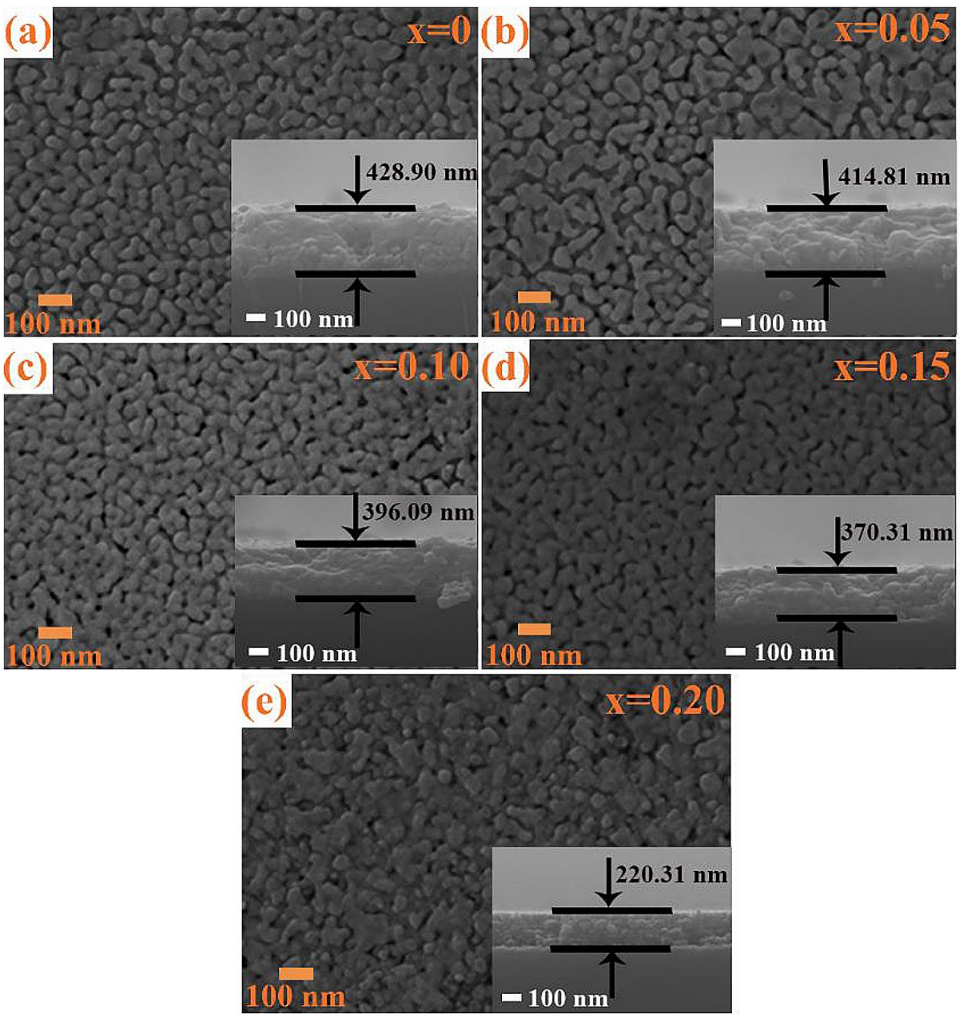

Fig. 2 Surface topographies of pure and doped $BiFeO_3$ thin films deposited on Si substrates. **a** Surface topography and thickness of $BiFeO_3$. **b** Surface topography and thickness of $BiFe_{0.95}Mn_{0.05}O_3$. **c** Surface topography and thickness of $BiFe_{0.90}Mn_{0.10}O_3$. **d** Surface topography and thickness of $BiFe_{0.85}Mn_{0.15}O_3$. **e** Surface topography and thickness of $BiFe_{0.90}Mn_{0.10}O_3$

reveals the uniform distribution of Mn dopant in the $BiFeO_3$ host for $BiFe_{0.80}Mn_{0.20}O_3$ thin film.

In addition, in order to ensure the crystallinity, particle size/shape and their distribution in the original and doped films, TEM measurements are carried out. The TEM images of $BiFeO_3$ with 10% Mn-doped films are showed in Fig. 3. In these images, the results show that the size of Mn-doped particles is uniform, the degree of agglomeration is high and the size is small, which is the same as SEM analysis results. The HRTEM image of the sample is shown in Fig. 3a, b, which show the high crystalline phases of the samples with plane spacing (d) of 0.402 and 0.396 nm, respectively.

In previous study, the deviation between known and oxidimetric measurements results in the fluctuation of valence states of Fe ions (+3 to +2 states) in $BiFeO_3$ [12]. Poor ferromagnetic properties of pure $BiFeO_3$ due to the reduction of Fe^{3+} to oxygen vacancies generated by volatilization of Fe^{2+} and Bi^{3+} [20]. For the sake of identifying the origin of the defects of the films, all thin films detailed XPS measurements are also carried out. The XPS survey spectra of $BiFeO_3$, $BiFe_{0.95}Mn_{0.05}O_3$, $BiFe_{0.90}Mn_{0.10}O_3$, $BiFe_{0.85}Mn_{0.15}O_3$ and $BiFe_{0.80}Mn_{0.20}O_3$ thin film have been recorded from 0 to 900 eV (Fig. 4f). For un-doped $BiFeO_3$, The emission peaks of $Bi4f_{7/2}$ and $Bi4f_{5/2}$ appear at 158.8 eV and 163.5 eV, respectively in Fig. 4f. The existence of this double peak indicates that there is no bismuth in the original sample, and bismuth ions exist in the trivalent oxidation state [21]. From Fig. 4f, we can see that as the doping concentration of Mn increases, the intensity of $Mn2p_{3/2}$ and $Mn2p_{1/2}$ peak gradually increases, indicating that Mn is successfully incorporated into $BiFeO_3$ thin film. Figure 4a–e show the XPS spectra fitting analysis of the Fe2p for pure, $BiFe_{0.90}Mn_{0.10}O_3$, $BiFe_{0.85}Mn_{0.15}O_3$ and $BiFe_{0.80}Mn_{0.20}O_3$ thin film, where binding energies were aligned with respect to the C1s peak (284.8 eV). The peak value of 710.9 eV is $Fe2p_{3/2}$ of Fe^{3+}. The peak value of 724.8 eV is $Fe2p_{1/2}$ of Fe^{3+} [22]. The results show that the $Fe2p_{3/2}$ peak of Fe^{2+} occurs at 709 eV. Although no peak was observed at 709 eV, the peak at 710.9 eV indicated that there was a certain amount of Fe^{2+} in un-doped $BiFeO_3$ [23]. In addition, the satellite peak of Fe^{3+} appeared above the main $2P_{3/2}$ peak, which further confirmed the existence of Fe^{3+} in the samples [24]. The XPS of the Mn2p peaks is shown in supplementary Figure S2. In $BiFe_{0.80}Mn_{0.20}O_3$ thin film, the binding energy of the main peak is 641.8 eV, and a shoulder peak lower than this energy can be observed. This peak comes from a small amount of Mn^{2+} (642.2 eV). It can be observed that the peak intensity increases with the increase of Mn doping concentration. In our experiment, since the Mn element is derived from $Mn(NO_3)_2$, divalent Mn ions will occupy a hole and become trivalent Mn ions. The results show that the substitution of Mn reduces the oxygen-related defects, which is consistent with the results of other Mn-doped $BiFeO_3$ samples [25]. At the same time, XPS results also support the reason why the $BiFe_{0.80}Mn_{0.20}O_3$ thin film in SEM results is denser.

In order to study the magnetic properties of pure, $BiFe_{0.95}Mn_{0.05}O_3$, $BiFe_{0.90}Mn_{0.10}O_3$, $BiFe_{0.85}Mn_{0.15}O_3$ and $BiFe_{0.80}Mn_{0.20}O_3$ thin films at normal atmospheric temperature, the VSM is used to measure the magnetization. The field-dependent magnetization (M–H) loop at normal atmospheric temperature is shown in Fig. 5a–e, which clearly indicates the ferromagnetism of the thin films. The value of saturation magnetization (MS) is determined by the node increment of two straight lines drawn from the high and low magnetic field positions of the M-H hysteresis loop. The coercive field (Hc) and Ms of all films are calculated as shown in Fig. 5f. The magnetization of the thin films increases with the Mn content increase at normal atmospheric temperature. Additionally, the Hc and Ms increase from Hc = 68 Oe (Oersted) and Ms = 10.2 emu/cm^3 for the $BiFeO_3$ thin film to Hc = 162 Oe and Ms = 83.5 emu/cm^3 for the 20 mol. % Mn–$BiFeO_3$ thin film, respectively, at normal atmospheric temperature. Our results can compare with the latest research on $BiFeO_3$ thin film. R.R. Awasthi et al. had

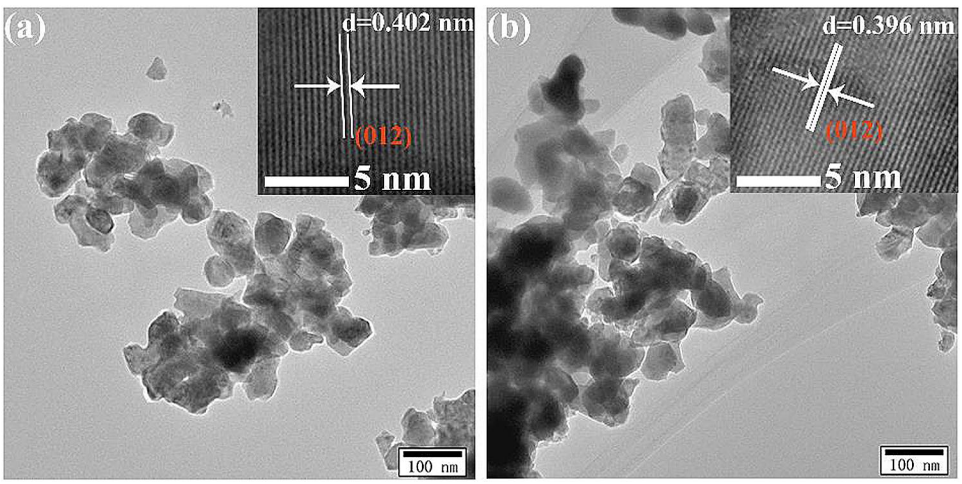

Fig. 3 TEM images for **a** pure $BiFeO_3$ and **b** $BiFe_{0.90}Mn_{0.10}O_3$ thin films

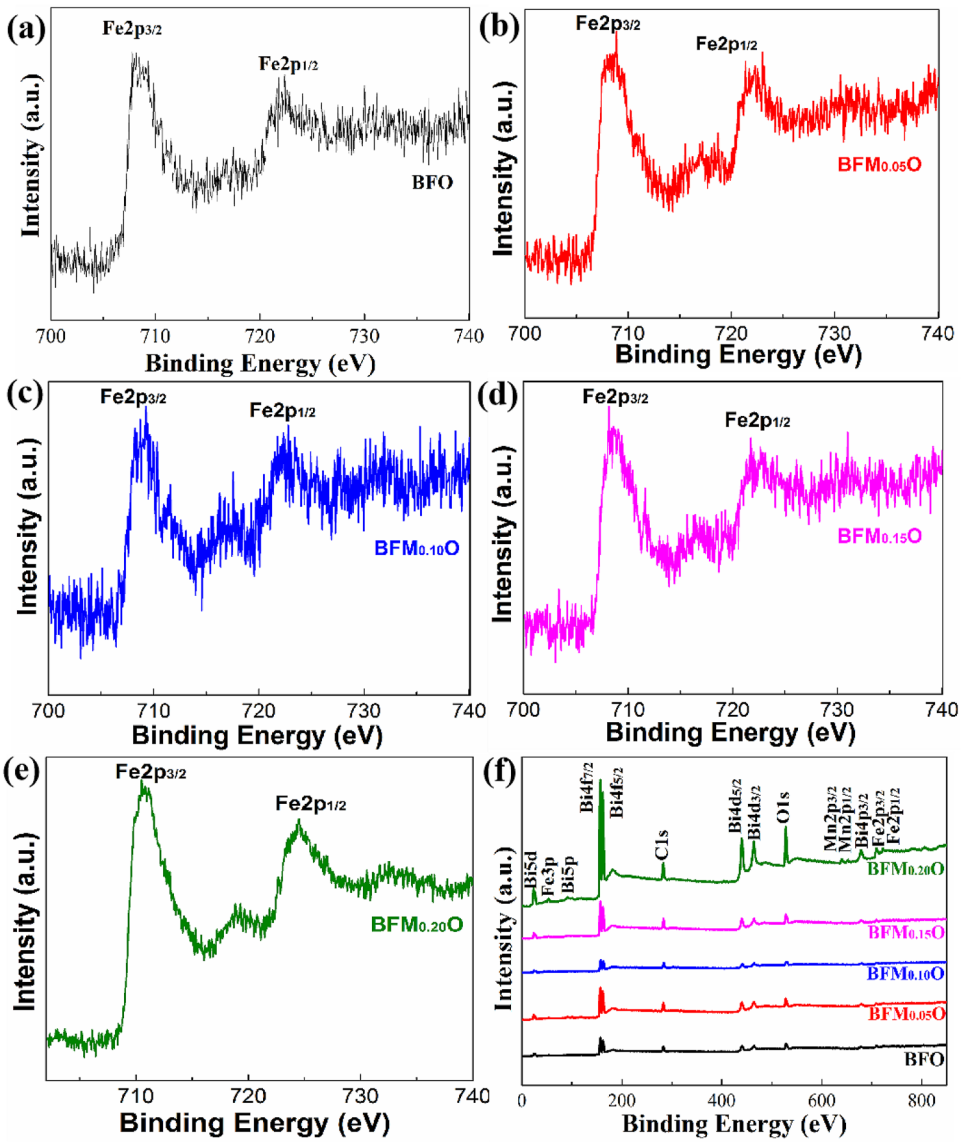

Fig. 4 XPS spectra of the as-annealed $BiFeO_3$, $BiFe_{0.95}Mn_{0.05}O_3$, $BiFe_{0.90}Mn_{0.10}O_3$, $BiFe_{0.85}Mn_{0.15}O_3$ and $BiFe_{0.80}Mn_{0.20}O_3$ thin films. **a**–**e** XPS spectra of the as-annealed $BiFeO_3$, $BiFe_{0.95}Mn_{0.05}O_3$, $BiFe_{0.90}Mn_{0.10}O_3$, $BiFe_{0.85}Mn_{0.15}O_3$ and $BiFe_{0.80}Mn_{0.20}O_3$ thin films in the binding energy regions of Fe2p. **f** XPS wide range spectra of all thin films

observed the Ms and Mr of Mn-doped $BiFeO_3$ thin film were 1.75 emu/cm^3 and 0.125 emu/cm^3, respectively [26]. Furthermore, Ren et al. reported the Mn and Cu co-substitution in $BiFeO_3$ thin films induced the Ms of 6.2 emu/cm^3 by a simple chemical solution deposition technique [27].

The observed magnetic behavior in $BiFeO_3$, $BiFe_{0.95}Mn_{0.05}O_3$, $BiFe_{0.90}Mn_{0.10}O_3$, $BiFe_{0.85}Mn_{0.15}O_3$ and $BiFe_{0.80}Mn_{0.20}O_3$ thin films may have some contributions [28]. That is as following. (i) As shown in Fig. 6a, b, the decrease of particle size (< 62 nm) destroys the spiral spin structure partially superimposed on the ordered structure of $BiFeO_3$ antiferromagnetic (AFM). The incomplete spiral structure leads to the non-complementary magnetic spin between two adjacent sublattices, which leads to the weakening of local magnetization [13]. Due to the influence of the magnetic field, the reorientation of the antiferromagnetic tilt arrangement spins of iron ions will increase the non-compensated spins to produce the total magnetization [29]. (ii) The increase of spin angle on the surface of nanoparticles, large surface volume ratio of nanoparticles can enhance the magnetization [30]. (iii) The magnetization may also enhance with magnetic Mn-substitutions as these substitutions increases the magnetic super exchange interaction among the Fe^{3+} cations. There are three main factors affecting the mechanism: the distances of Fe^{3+}–O^{2-}–Mn^{2+}, the number of Fe^{3+}-Mn^{2+} magnetic ion pairs and oxygen ions as the Fe^{3+}–O^{2-}–Mn^{2+} interaction medium [31].

5 Conclusions

In this paper, we have synthesized and extensively characterized the pure, $BiFe_{0.95}Mn_{0.05}O_3$, $BiFe_{0.90}Mn_{0.10}O_3$, $BiFe_{0.85}Mn_{0.15}O_3$ and $BiFe_{0.80}Mn_{0.20}O_3$ thin films via a

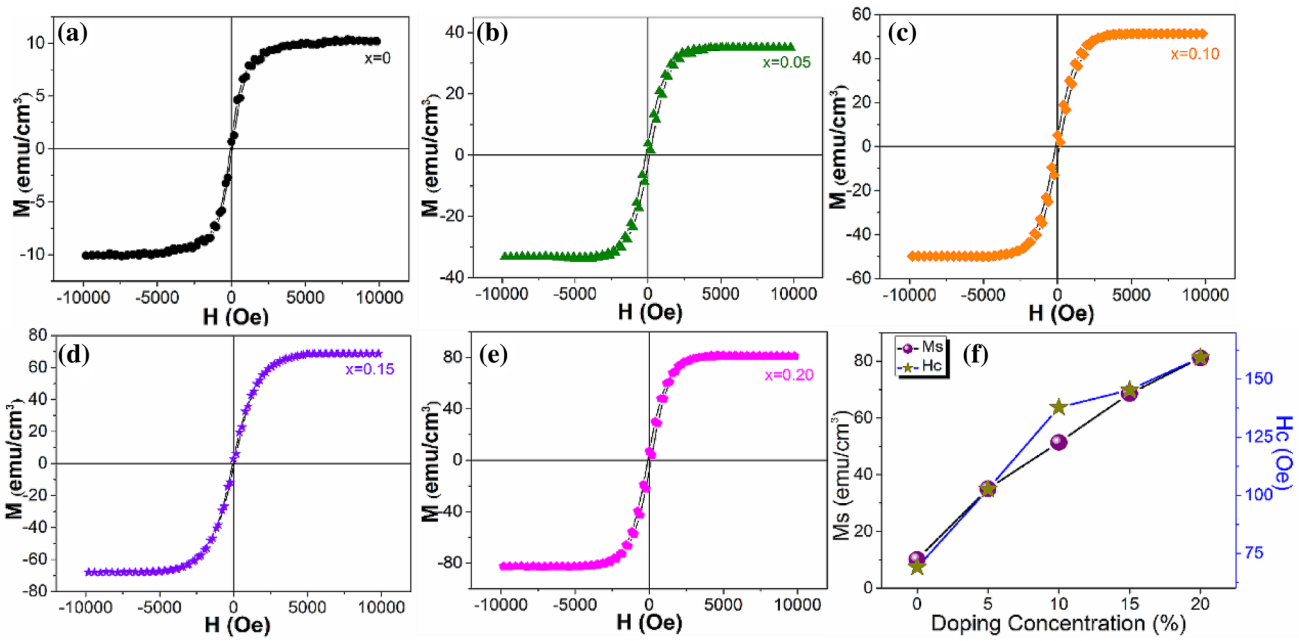

Fig. 5 Magnetic property of $BiFeO_3$, $BiFe_{0.95}Mn_{0.05}O_3$, $BiFe_{0.90}Mn_{0.10}O_3$, $BiFe_{0.85}Mn_{0.15}O_3$ and $BiFe_{0.80}Mn_{0.20}O_3$ thin films. **a–e** Magnetic field-dependent magnetization at normal atmospheric temperature for $BiFe_{1-x}Mn_xO_3$ ($x=0$, 0.05, 0.10, 015, 0.20) thin films. **f** Saturation magnetization and coercivity of sample depend on Mn^{2+} ion ($x=0$, 0.05, 0.10, 0.15, 0.20)

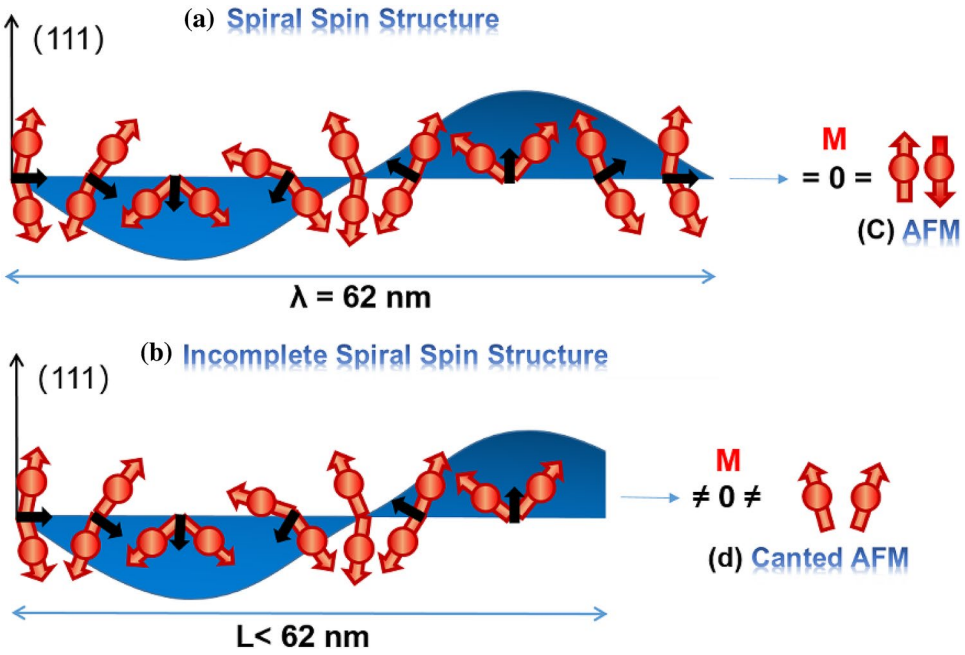

Fig. 6 **a** Full spiral spin structure. **b** Incomplete spiral spin structure. **c** AFM spin. **d** Canted AFM spin

sol–gel process on silicon substrates. We analyzed the pristine and doped $BiFeO_3$ thin films structures with XRD, with further processing. XRD and Rietveld analysis showed that the typical rhombohedral-*R3c* ($BiFeO_3$) was transformed into orthorhombic-*Pbmn* ($BiFe_{0.80}Mn_{0.20}O_3$). XPS analysis showed that the content of Fe^{3+} in $BiFe_{1-x}Mn_xO_3$ thin film was increased. It's worth to point out that the magnetic properties are highly influenced by the incorporation of Mn. $BiFe_{0.80}Mn_{0.20}O_3$ thin film has the highest magnetization of Ms ~ 83.5 emu/cm^3 and Hc ~ 162 Oe, which may be due to the new super exchange between Fe^{3+}–O^{2-}–Mn^{2+} ions, the increase of spin angle on the surface of nanoparticles and the change of spatial modulation spin structure caused by the structural transformation. We provide a theoretical basis for

the future application of multiferroic materials in memory devices, sensors and so on in this paper.

Acknowledgements The authors would like to acknowledge the financial support by National Natural Science Foundation of China under Grants 11705119 and 61401525, Science and Technology Planning Project of Jilin City named Research on Key Technologies of wireless wearable health monitoring equipment, Doctoral Initiated Research Foundation Project under Grants BSKJ201822, BSKJ201820 and BSKJ201821, Natural Science Foundation of Guangdong Province under Grant 2017A030310142, Scientific Research Planning Project of Education Department of Jilin Province under Grant JJKH20200180KJ.

Author contributions MZ: Resources, Visualization, Writing-review and editing, Writing-original draft preparation. JL: Formal analysis, Data curation, Supervision. CW: Investigation, Project administration, Funding acquisition. XA: Investigation, Conceptualization. YW: Validation, Methodology. WX: Methodology. LG: Resources, Funding acquisition, Writing-review and editing.

Compliance with ethical standards

Conflict of interest We declare that we have no financial and personal relationships with other people or organizations that can inappropriately influence our work, there is no professional or other personal interest of any nature or kind in any product, service and/or company that could be construed as influencing the position presented in, or the review of, the manuscript entitled.

References

1. W. Eerenstein, N.D. Mathur, J.F. Scott, Multiferroic and magnetoelectric materials. Nature **442**, 759–765 (2006)
2. S.W. Cheong, M. Mostovoy, Multiferroics: a magnetic twist for ferroelectricity. Nat. Mater. **6**, 13–20 (2007)
3. C.S. Watson, C. Hollar, K. Anderson, W.B. Knowlton, P. Müllner, Magnetomechanical four-state memory. Adv. Funct. Mater. **23**, 3995–4001 (2013)
4. P.M. Razad, K. Saravanakumar, V. Ganesan, V.R. Reddy, R.J. Choudhary, K. Jeyadheepan, K. Mahalakshmi, Ferromagnetic ordering in nickel doped $BiFeO_3$ nanostructured thin films. J. Mater. Sci.-Mater. El. **30**, 18306–18314 (2019)
5. Y. Li, H.J. Yang, X.H. Hao, N.N. Sun, M.S. Cao, Enhanced electromagnetic interference shielding with low reflection induced by heterogeneous double-layer structure in $BiFeO_3$/$BaFe_7(MnTi)_{2.5}O_{19}$ composite. J. Alloy. Compd. **772**, 99–104 (2019)
6. V.M. Gaikwad, S.A. Acharya, Investigation on magnetic behaviour of $BiFeO_3$: SPIN glass view point. Adv. Mat. Lett. **5**, 157–160 (2014)
7. J. Xu, D. Gao, X. Wang, X. Zhou, B. Zhu, X. Qi, D. Sekulic, P. He, Z. Li, T. Lin, S. Zhang, Joining ZnS ceramics by using $PbTiO_3$ doped PbO–B_2O_3–ZnO. J. Mater. Sci. (2020). https://doi.org/10.1007/s10853-020-04660-0
8. F. Xue, L. Tang, G. Jian, W. Li, Sintering and fatigue properties of Pb and La co doped $BiFeO_3$ multiferroics. J. Mater. Sci. Mater. Electron. **28**, 9344–9350 (2017)
9. T. Wang, S.-H. Song, M.-L. Qing Ma, J.-J. Tan, Highly improved multiferroic properties of Sm and Nb co-doped $BiFeO_3$ ceramics prepared by spark plasma sintering combined with sol–gel powders. J. Alloy. Compd. **795**, 60–68 (2019)
10. I.M. Reaney, I. MacLaren, L. Wang, B. Schaffer, A. Craven, K. Kalantari, I. Sterianou, S. Miao, S. Karimi, D.C. Sinclair, Defect chemistry of Ti-doped antiferroelectric $B_{i0.85}Nd_{0.15}FeO_3$. Appl. Phys. Lett. **100**, 182902 (2012)
11. W. Mao, Y. Xa Li, X. Li, Y. Wang, Y. Wang, X. Ma, T. Feng, J.Y. Yang, Structural phase transition and multiferroic properties of single-phase $Bi_{1-x}Er_xFe_{0.95}Co_{0.05}O_3$. Mater. Lett. **97**, 56–58 (2013)
12. Q.-Y. Rong, W.-Z. Xiao, G. Xiao, A.-M. Hu, L.-L. Wang, Magnetic properties in $BiFeO_3$ doped with Cu and Zn first-principles investigation. J. Alloy. Compd. **674**, 463–469 (2016)
13. W.W. Mao, X.F. Wang, L. Chu, Y.Y. Zhu, Q. Wang, J. Zhang, J.P. Yang, X.A. Li, W. Huang, Simultaneous enhancement of magnetic and ferroelectric properties in Dy and Cr co-doped $BiFeO_3$ nanoparticles. Phys. Chem. Chem. Phys. **18**, 399–6405 (2016)
14. V. Sharma, R.K. Ghosh, B.K. Kuanr, Investigation of room temperature ferromagnetism in transition metal doped $BiFeO_3$. J. Phys. Condens. Matter **31**, 395802 (2019)
15. M. Abushad, W. Khan, S. Wasi, S. Naseem, M. Husain, A.A. Nadeem, Influence of Mn doping on microstructure, optical, dielectric and magnetic properties of $BiFeO_3$ nanoceramics synthesized via sol–gel method. Ceram. Int. **45**, 7437–7445 (2019)
16. V.A. Khomchenko, D.V. Karpinsky, I.O. Troyanchuk, V.V. Sikolenko, D.M. Toebbens, M.S. Ivanov, M.V. Silibin, R. Rai, Polar-antipolar transition and weak ferromagnetism in Mn-doped. J. Phys. D-Appl Phys **51**, 165001 (2018)
17. S. Zhang, X. Xu, T. Lin, P. He, Recent advances in nano-materials for packaging of electronic devices. J. Mater. Sci.-Mater. Electron. **30**, 13855–13868 (2019)
18. W. Mao, X. Wang, Y. Han, X. Li, Y. Li, Y. Wang, X. Ma, T. Feng, J. Yang, W.H. Yang, Effect of Ln (Ln=La, Pr) and Co co-doped on the magnetic and ferroelectric properties of $BiFeO_3$ nanoparticles. J. Alloy. Compd. **584**, 520–523 (2014)
19. P. Tang, D.H. Kuang, S.H. Yang, Y.L. Zhang, Structural, morphological and multiferroic properties of the hydrothermally grow gadolinium (Gd) and manganese (Mn) doped sub-micron bismuth ferrites. J. Alloy. Compd. **622**, 194–199 (2015)
20. G.L. Yuan, S.W. Or, H.L.W. Chan, Z.G. Liu, Raman scattering spectra and ferroelectric properties of $Bi_{1-x}Nd_xFeO_3$ (x=0−0.2 multiferroic ceramics. J. Appl. Phys. **101**, 024106–024110 (2007)
21. P. Suresh, P.D. Babu, S. Srinath, Role of (La, Gd) co-doping on the enhanced dielectric and magnetic properties of $BiFeO_3$. Ceram. Inter. **42**, 4176–4184 (2016)
22. W.B. Luo, J. Zhu, Y.R. Li, X.P. Wang, D. Zhao, J. Xiong, Y. Zhang, Effects of chemical fluctuations on microstructures and properties of multiferroic $BiFeO_3$ thin films. Appl. Phys. Lett. **91**, 082501 (2007)
23. C.M. Raghavan, W.K. Jin, S.K. Sang, Effects of Ho and Ti Doping on structural and electrical properties of $BiFeO_3$ thin films. J. Am. Ceram. Soc. **97**, 235–240 (2014)
24. Y. Ren, X. Zhu, C. Zhang, J. Zhu, J. Zhu, D. Xiao, High stable dielectric permittivity and low dielectric loss in sol–gel derived $BiFeO_3$ thin films. Ceram. Int. **40**, 2489–2493 (2014)
25. Q.Y. Xu, Y. Sheng, M. Khalid, Y.Q. Cao, Y.T. Wang, X.B. Qiu, W. Zhang, M.C. He, S.B. Wang, S.Q. Zhou, Q. Li, D. Wu, Y. Zhai, W.Q. Liu, P. Wang, Y.B. Xu, J. Du, Magnetic interactions in $BiFe_{0.5}Mn_{0.5}O_3$ films and $BiFeO_3$/$BiMnO_3$ superlattices. Sci. Rep. **5**, 9093 (2015)
26. R.R. Awasthi, B. Das, Structural transition and tunable optical, morphological and magnetic properties of Mn-doped $BiFeO_3$ films. Optic **194**, 162973 (2019)
27. G.H. Dong, G.Q. Tan, Y.Y. Luo, W.L. Liu, A. Xia, H.J. Ren, Charge defects and highly nhanced multiferroic properties in Mn and Cu co-doped $BiFeO_3$ thin films. Appl. Urf. Sci. **305**, 55–61 (2014)

28. S. Mukherjee, R. Gupta, A. Garg, V. Bansal, S. Bhargava, Influence of Zr doping on the structure and ferroelectric properties of $BiFeO_3$ thin films. J. Appl. Phys. **107**, 123535 (2010)
29. T.J. Park, G.C. Papaefthymiou, A.J. Viescas, A.R. Moodenbaugh, S.S. Wong, Sizedependent magnetic properties of single-crystalline multiferroic $BiFeO_3$ nanoparticles. Nano Lett. **7**, 766–772 (2007)
30. M.E. Castillo, V.V. Shvartsman, D. Gobeljic, Y. Gao, J. Landers, H. Wende, D.C. Lupascu, Effect of particle size on ferroelectric and magnetic properties of $BiFeO_3$ nanopowders. Nanotechnology **24**, 355701 (2013)
31. J.Y. Chen, W. Yao, D. Yuan, Combined effects of Bi deficiency and Mn substitution on the structural transformation and functionality of $BiFeO_3$ films. J. Appl. Phys. **116**, 174102 (2014)